*Intelligent and Converged Networks*
**2021, 2(1): 50–65**

**ISSN 2708-6240**
**DOI: 10.23919/ICN.2020.0024**

# Performance analysis of a low-complexity nonorthogonal multiple access scheme in visible light communication downlinks using pulse modulations

**Jian Song, Tian Cao*, and Hongming Zhang***

**Abstract:** Although Successive Interference Cancellation (SIC) decoding is widely adopted in Nonorthogonal Multiple Access (NOMA) schemes for the recovery of user data at acceptable complexity, the imperfect SIC would cause Error Propagation (EP), which can severely degrade system performance. In this work, we propose an SIC-free NOMA scheme in pulse modulation based Visible Light Communication (VLC) downlinks, including two types of users with different data rate requirements. Low bit-rate users adopt on-off keying, whereas high bit-rate ones use Multiple Pulse Position Modulation (MPPM). The soft decision decoding scheme is exploited by high bit-rate users to decode MPPM signals, which could fundamentally eliminate the detrimental effect of EP; the scheme is also easier and faster to execute compared with the conventional SIC decoding scheme. Expressions of the symbol error rate and achievable data rate for two types of users are derived. Results of the Monte Carlo simulation are provided to confirm the correctness of theoretical results.

**Key words:** visible light communication; nonorthogonal multiple access; error propagation; on-off keying; multiple pulse position modulation; symbol error rate; achievable data rate

## 1 Introduction

With the rapid development of Light-Emitting Diodes (LEDs), the LED-enabled Visible Light Communication (VLC) technique, which modulates the intensity of optical sources to transmit information at a rate much faster than the response time of the human eyes[1], has attracted considerable attention. LED-enabled VLC systems can provide data transmission services by simultaneously exploiting existing LED-based illumination infrastructure[2]. This type of communication system can be realized by connecting LED lamps to a modem through cables or by directly adopting an integrated solution of VLC and Power Line Communication (PLC)[3]. In addition, VLC has many attractive features, such as ultrawide spectral bands, license-free spectra, no electromagnetic interference, secure transmission, and low energy consumption[4,5]. Therefore, VLC is recognized as a promising and competitive candidate of the Sixth-Generation (6G) communications and beyond[6,7].

At present, the modulation bandwidth of commercial white LEDs is only approximately 10 MHz, which limits the Achievable Data Rate (ADR) of VLC systems. To improve this situation, some techniques, such as equalization[8], spatial diversity[9], and more efficient multiple access schemes[10], have been proposed and

• Jian Song and Hongming Zhang are with Beijing National Research Center for Information Science and Technology (BNRist), Department of Electronic Engineering, Tsinghua University, Beijing 100084, China, and also with Key Laboratory of Digital TV System of Guangdong Province and Shenzhen City, Research Institute of Tsinghua University in Shenzhen, Shenzhen 518057, China. E-mail: jsong@tsinghua.edu.cn; zhhm@tsinghua.edu.cn.

• Tian Cao is with Beijing National Research Center for Information Science and Technology (BNRist), and Department of Electronic Engineering, Tsinghua University, Beijing 100084, China. E-mail: caot19@mails.tsinghua.edu.cn.

* To whom correspondence should be addressed.

Manuscript received: 2020-11-03; accepted: 2020-12-08

studied. Traditionally, multiple access schemes, which are classified as Orthogonal Multiple Access (OMA) schemes, always assign orthogonal resources, e.g., time, frequency, and space, to users to avoid mutual interference. In contrast to OMA schemes, recently proposed Nonorthogonal Multiple Access (NOMA) schemes are designed to allocate the same orthogonal resources to different users simultaneously. That is, each user could share the identical frequency, time, and spatial resources in NOMA-based systems. NOMA schemes could be realized in the power or code domain[11]. The latter realization of NOMA is similar to the code-division multiple access technique, except that it prefers using low-density sequences[12]. In this work, we mainly focus on the power-domain NOMA scheme because it has lower computational complexity and is more suitable for VLC systems compared with the code-domain one[13, 14]. Unless otherwise stated, the term "NOMA" exclusively stands for the power-domain NOMA scheme hereinafter. In this type of multiple access scheme, Superposition Coding (SC) and Successive Interference Cancellation (SIC) are commonly conducted at the transmitter and receiver, respectively. Specifically, in accordance with the channel quality, all users are ranked from the worst to the best. The user under the worst channel condition is allocated to the highest transmitting power and vice versa. Therefore, different transmitting power levels of signals from the highest to the lowest are orderly assigned to users with channel quality from the worst to the best at first. Then those signals are superposed in the power domain and emitted via the transmitting antennas at base stations. At receiver sides, each user, according to the order of users, must subtract the former users' reconstructed signals successively after those signals are successfully received and decoded from the combined signal; then it decodes its own signal by treating the rest users' signals as interference. This kind of NOMA could achieve more equitable user fairness than conventional OMA schemes[11].

### 1.1 Related work

In recent years, the subject of applying NOMA schemes to VLC systems has remained an open topic and has been widely studied theoretically or experimentally. Here we roughly categorize the reported works in terms of their main contributions into five groups, including (1) power allocation, (2) cooperation with OMA and user grouping, (3) NOMA with various Orthogonal Frequency-Division Multiplexing (OFDM) schemes, (4) physical-layer security, and (5) error performance and mitigation of Error Propagation (EP).

At present, power allocation schemes proposed for NOMA-VLC systems can be classified into two types: channel gain determined and optimization method based schemes. Specifically, for channel gain determined schemes, Marshoud et al. proposed a power allocation strategy named Gain Ratio Power Allocation (GRPA)[15]. Later, Chen et al. proposed the Normalized Gain Difference Power Allocation (NGDPA) scheme for Multiple-Input Multiple-Output (MIMO) NOMA-VLC systems by exploiting the optical channel gain difference between two users[16]. Inspired by NGDPA, Wang et al. proposed Normalized Logarithmic GRPA (NLGRPA), which exhibits an improvement of more than 55% and 33% compared with the GRPA and NGDPA in the considered MIMO NOMA-VLC systems[14]. For optimization method based power allocation schemes, researchers attempt to find the optimal or suboptimal power allocation factor to maximize the sum rate or minimize the error probability. In Ref. [17], the authors maximized the sum throughput of NOMA-VLC systems, considering user fairness and unique intensity constraints for optical signals. Fu et al. proposed an enhanced power allocation algorithm to maximize the sum of data rates and minimize the subcarrier loss rate of the system by considering user- and subcarrier-level power allocation in OFDM-based NOMA-VLC systems[18]. Li et al. proposed an optimal power allocation strategy based on multi-factor control for an indoor NOMA-VLC scenario with multiple users, aiming to maximize the total system capacity subject to the Quality of Service (QoS) requirement, fairness, and eye security of each user simultaneously[19]. By taking the power line as a backbone feed for VLC systems, Feng et al. proposed a joint PLC-VLC power allocation strategy to maximize the sum throughput of a PLC-VLC network[20].

Although NOMA is preferable because it allows users to share identical time, frequency or spatial resources, supporting numerous users in one realization

of NOMA scheme is impractical[13]. Instead, dividing users in NOMA-VLC systems into different groups is more advisable. NOMA is further conducted within each group, and conventional OMA could be implemented among groups. This idea also refers to hybrid OMA/NOMA networking. In Ref. [21], the combination of NOMA and Orthogonal Frequency-Division Multiple Access (OFDMA) was proposed in the downlink and uplink of VLC networks, and the corresponding Bit-Error Rate (BER) performance was studied experimentally. Later, Abumarshoud et al. proposed the intelligent dynamic multiple access selection scheme, which could realize an adaptive configuration of the available multiple access modes, including OMA, NOMA, and hybrid OMA/NOMA[22]. Furthermore, how to group users in VLC systems must be addressed. In some reported works, user grouping is also called user pairing. In Ref. [23], the authors investigated the performance of system coverage probability and ergodic sum rate in NOMA-VLC systems upon guaranteed QoS and opportunistic best-effort assumptions, respectively. In Ref. [24], the authors considered the height of users and studied the problem of user grouping in 3D NOMA-VLC scenarios.

Recently, some efficient OFDM schemes combined with NOMA have been studied to improve the performance of NOMA-VLC systems. Nauryzbayev et al. investigated the BER performance of NOMA-VLC systems with Spectrally and Energy Efficient OFDM (SEE-OFDM)[25]. Then they further derived an exact expression of the outage probability for SEE-OFDM in a NOMA-VLC network[26]. Li et al. proposed a Hierarchical Predistorted Layered Asymmetrically Clipped Optical OFDM (HPD-LACO-OFDM) scheme for NOMA-VLC systems[27]. In addition, they experimentally compared the BER performance of the Directed Current biased Optical (DCO)-OFDM, the LACO-OFDM, and the HPD-LACO-OFDM schemes in two-user NOMA-VLC systems. In Ref. [28], the authors proposed an offset quadrature amplitude modulation/OFDM, which also refers to the filter bank multicarrier, combined with a NOMA scheme. Adnan et al. investigated a NOMA-VLC system with non-Hermitian symmetry Inverse Fast Fourier Transform (IFFT)/FFT size-efficient OFDM via experiments[29] and simulations[30].

Physical-layer security approaches originate from the fundamentals of information theory, focus on the secrecy capacity of the channel, and exploit the channel characteristics to hide information from illegitimate users, without dependence on upper-layer cryptographic mechanisms. Some progress has been made regarding physical-layer security in NOMA-VLC systems. In Ref. [31], Zhao et al. systematically investigated the secrecy outage probability performance under single and multiple eavesdropper conditions and derived the corresponding expressions. In Ref. [32], Yang et al. proposed a NOMA-VLC system with a two-level chaotic encryption scheme. The results showed that this scheme can guarantee the security of legitimate users against eavesdroppers and privacy among all legitimate users.

As a basic metric of communication systems, error performance is indispensable in assessing the capability of NOMA-VLC systems. SIC is commonly adopted at the receiver to recover and decode signals. To simplify the performance analysis of NOMA-VLC systems, most reported works assume that the perfect SIC has been achieved. However, the user in NOMA schemes must successively cancel the former users' signal before decoding its own signal; thus, the errors from the imperfect decoding of former users' data may exert adverse effects on decoding the user's own signal. This problem refers to EP, which can deteriorate the error performance of NOMA-VLC systems. Lin et al. experimentally studied the BER performance of an MIMO-NOMA-VLC system with single carrier transmission and frequency domain SIC[33]. Marshoud et al. derived the BER expressions of NOMA-VLC systems with On-Off Keying (OOK) modulation adopted under perfect, noisy, and outdated channel state information conditions, respectively[34]. In Ref. [35], Liu et al. derived closed-form BER expressions for M-ary phase shift keying, M-ary pulse amplitude modulation, and M-ary quadrature amplitude modulation in NOMA-VLC systems with two users. To mitigate the effect of EP on the error performance of NOMA-VLC systems, some approaches have been proposed in recent works. Symmetric SC and symmetric SIC

decoding schemes for the downlink of NOMA-based VLC systems with Quadrature Amplitude Modulation (QAM) were proposed in Ref. [36], wherein the authors experimentally demonstrated that their solution could alleviate approximately 90% demodulation errors caused by EP. Later, for the VLC downlink, Chen et al. proposed a Gray-coded QAM-based NOMA scheme, where constellation partitioning coding and uneven constellation demapping are proposed and utilized at the transmitter and receiver, respectively[37]. Given that SIC is not implemented in this NOMA scheme anymore, the effect of EP can be thoroughly eliminated. In Ref. [38], Shi et al. proposed the subcarrier pairwise coding scheme in NOMA-VLC systems with OFDM adopted. This scheme was experimentally demonstrated, and the corresponding results showed that the system performance can be remarkably improved. For OOK-based NOMA-VLC systems, we proposed an adjustable bit-rate SC scheme at the transmitter and sample-and-sum SIC scheme at the receiver to mitigate the effect of EP[39]. In our solution, the bit-rate factor was introduced to adjust the bit rate of each user. Specifically, more transmitting power and lower bit rate are assigned to the user with lower channel gain, i.e., under the worse channel condition. Therefore, more than one sample of the data symbol could be obtained for this user within a bit interval. The process of summing those samples up would average the random noise, lower the BER, and thus reduce the probability of EP.

### 1.2 Motivation and contribution

The above investigations show that most EP mitigation approaches in NOMA-VLC systems are designed for QAM[36,37] or OFDM[38]. Given that VLC prefers Intensity Modulation and Direct Detection (IM/DD), pulse modulation schemes, such as OOK, pulse position modulation, and pulse width modulation, attract considerable attention and are widely implemented in VLC systems because of its low cost and simplicity[40,41]. Therefore, we attempt to design EP mitigation methods for NOMA-VLC systems with pulse modulation schemes[39].

Although the method proposed in Ref. [39] could effectively relieve the effect of EP on the error performance of NOMA-VLC systems, it cannot fundamentally eliminate this negative effect. In addition, in this method, the total instantaneous signal power of the higher bit-rate user is not constant during a bit interval of the lower bit-rate user because the information of the higher bit-rate user is uncertain. As a result, the sum of the sampled values in a bit interval of the lower bit-rate user randomly fluctuates, and the corresponding error performance further deteriorates. Later, we noticed that a Multiple Pulse Position Modulation (MPPM) symbol contains multiple slots, and the total transmitting power of those slots in one MPPM symbol is constant, which seems to be useful to solve this problem.

In practical VLC systems, all users can be divided into two types in terms of data rate requirements. High bit-rate users, such as mobile phones and laptops, are more likely located in places near LEDs to obtain enough illumination and are usually pivotal users. Thus, they are commonly under better channel conditions. By contrast, low bit-rate users, such as sensors and Internet of Things devices, are always mounted on the wall or furniture, maybe far away from LEDs under worse channel condition. In contrast to Ref. [39] where the bit rate was adjusted to mitigate the effect of EP, the present work naturally considers the existence of high and low bit-rate users in the VLC system and proposes a novel NOMA scheme for a two-user VLC system with pulse modulations, where the low bit-rate user adopts OOK and the high bit-rate user utilizes MPPM. Furthermore, Soft Decision Decoding (SDD) is introduced to decode the MPPM signal at the receiver of the high bit-rate user. Given that the SIC does not need to be implemented anymore, the proposed NOMA scheme fundamentally eliminates the effect of EP.

The detailed contributions of this study are listed as follows:

(1) We propose a novel NOMA scheme for a two-user VLC system with pulse modulations; this scheme could fundamentally eliminate the effect of EP.

(2) We derive the expressions of Symbol Error Rate (SER) and ADR for the low and high bit-rate users, respectively. The asymptotically approximated expressions for the probability of the number of wrongly decoded slots in one MPPM symbol are also provided in low and high Signal-to-Noise Ratio (SNR) regions;

and these expressions are critical in evaluating the ADR performance. The results of Monte Carlo (MC) simulation are provided to verify the correctness of theoretical results.

(3) We analyze the effect of SNRs and power allocation factors on SER performance and compare the SER results with those obtained from Ref. [39] and the SIC-based NOMA decoding scheme. Furthermore, we analyze the ADR of users and the sum rate of systems with different power allocation factors, SNRs, number of total slots, and number of pulsed slots in one MPPM symbol. In addition, the ADR performance of the proposed NOMA scheme is compared with that of conventional OMA schemes.

## 2 System model

A diagram of the two-user NOMA-VLC downlink is demonstrated in Fig. 1. An LED mounted on the ceiling (facing vertically downward) is used for dual purposes of illumination and data transmission. $\psi_{1/2}$ denotes the LED emission semi-angle. Two users, namely, User 1 (U1) and User 2 (U2) in Fig. 1, are considered here; each is equipped with a Photo Detector (PD) facing vertically upward. $\varphi_{\mathrm{c}}$ is the Half-Field Of View (HFOV) of PD. Considering that the average optical power of the Line-Of-Sight (LOS) link between the LED and the $k$-th user's PD ($k = 1, 2$) is much stronger than that of diffuse links in VLC channels, we exclusively consider the channel gain of the LOS link. In accordance with Ref. [34], the channel gain of the LOS link can be expressed as

$$h_k = \begin{cases} \dfrac{(\delta+1)\cos^{\delta}(\psi_k) A_k}{2\pi d_k^2} T(\varphi_k) \times \\ \quad g(\varphi_k)\cos(\varphi_k), 0 \leqslant \varphi_k \leqslant \varphi_{\mathrm{c}}; \\ 0, \qquad\qquad \varphi_k > \varphi_{\mathrm{c}} \end{cases} \tag{1}$$

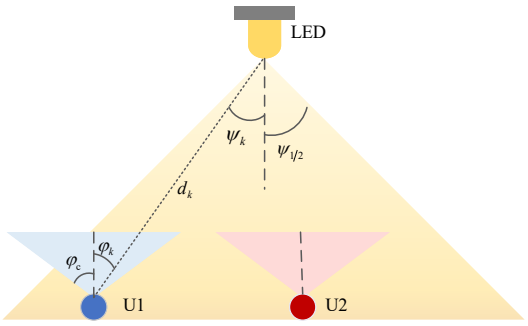


**Fig. 1 Channel model of the NOMA-VLC downlink with two users.**

where $A_k$ is the PD detection area of the $k$-th user; $d_k$ is the link distance between the LED and the $k$-th user; $\psi_k$ and $\varphi_k$ denote the angle of irradiance and the angle of incidence at the $k$-th user, respectively. The order of Lambertian emission is represented by $\delta = -\ln(2) / \ln\left(\cos\left(\psi_{1/2}\right)\right)$; $T(\varphi_k)$ and $g(\varphi_k)$ are the gain of optical filter and the optical concentrator, respectively. $g(\varphi_k)$ can be written as

$$g(\varphi_k) = \begin{cases} \dfrac{\rho^2}{\sin^2(\varphi_{\mathrm{c}})}, & 0 \leqslant \varphi_k \leqslant \varphi_{\mathrm{c}}; \\ 0, & \varphi_k > \varphi_{\mathrm{c}} \end{cases} \tag{2}$$

where $\rho$ denotes the reflective index of the optical concentrator.

Without loss of generality, we assume that U1 is a low bit-rate user and U2 is a high bit-rate user, just like the example in Fig. 1. Therefore, U1 uses OOK modulation, and U2 adopts $(M, N)$ MPPM, where $M$ is the number of total slots and $N$ is the number of pulsed slots, which also refer to the signal slots in one MPPM symbol. The symbol rates of OOK and MPPM are assumed to be the same, and all symbols are synchronized. The processes of the proposed NOMA scheme in the VLC downlink at the transmitter and receiver are illustrated in Fig. 2, in which we take $(5, 2)$ MPPM for U2 as an example. Signals of U1 and U2 are separately generated and then superposed in the power domain. Driven by the combined signal, the LED emits the intensity-modulated light, which is received by each user after propagation over the VLC channel. Let $\alpha$ denote the power allocation factor and $P_{\mathrm{t}}$ represent the average optical power of the LED. The average optical power of U1 is $P_1 = \alpha P_{\mathrm{t}}$, and that of U2 is $P_2 = (1-\alpha) P_{\mathrm{t}}$. OOK is adopted by U1; thus, the instantaneous optical power levels of U1's signal for bits "0" and "1" are 0 and $2P_1$, respectively. Given that $(M, N)$ MPPM is adopted by U2, the instantaneous optical power levels of U2's signal are 0 for unpulsed slots and $MP_2/N$ for pulsed slots. The PD of each user's receiver converts the received optical signal to an analog electrical signal. Then the analog electrical signals of U1 and U2 are sampled at a rate of $f_{\mathrm{s}}$, which is equal to the slot rate of MPPM. Afterward, U1 sums up the sampled values in a bit interval and uses Maximum Likelihood Decision (MLD) to decode the signal. U2

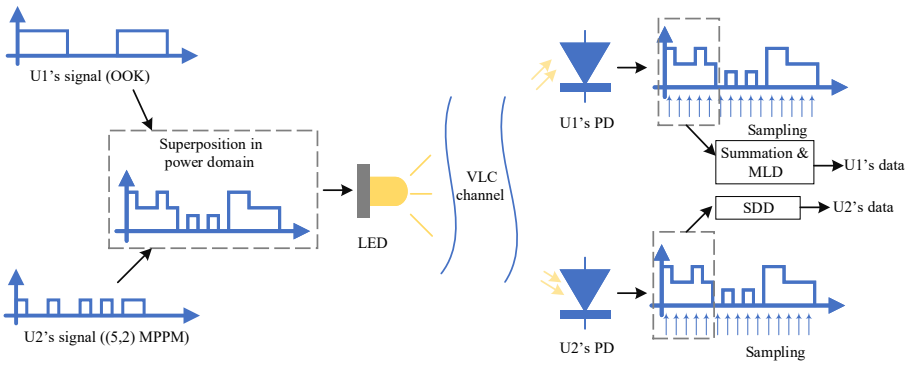


**Fig. 2 Graphical representation of two-user NOMA scheme in the downlink of VLC, where low bit-rate user (U1) uses OOK and high bit-rate user (U2) adopts (5, 2) MPPM.**

handles those sampled values by SDD scheme, where the decoder selects the largest $N$ sampled values from $M$ sampled values of a symbol block, and then regards those $N$ slots as pulsed slots. Hence, SIC decoding does not need to be implemented anymore. Compared with the traditional SIC-based NOMA scheme, the proposed NOMA scheme is easier and faster to perform. Without loss of generality, the output values of the sampler are assumed to be independent from each other. Therefore, the output of sampler at the $k$-th user can be expressed as

$$y_k = \begin{cases} \frac{h_k MRP_2}{N} + n_k, & \text{pulsed slot } (x_1 = 0); \\ n_k, & \text{unpulsed slot } (x_1 = 0); \\ 2h_k RP_1 + \frac{h_k MRP_2}{N} + n_k, & \text{pulsed slot } (x_1 = 1); \\ 2h_k RP_1 + n_k, & \text{unpulsed slot } (x_1 = 1) \end{cases} \tag{3}$$

where $x_1$ is the bit transmitted for U1; $R$ denotes the responsivity of the PD. $n_k$ represents the zero-mean additive white Gaussian noise with variance $\sigma^2_{n_k} = N_0/2$, where $N_0$ is the power spectral density. In practical VLC systems, if a narrow spectral filter is used at receiver, the ambient light and the signal-dependent shot noise could be neglected; and the thermal noise from the circuitry of the receiver is dominant[18,42,43]. Therefore, we assume that the noise in the considered NOMA-VLC system is normally distributed and signal-independent. The average electrical SNR at the receiver of the $k$-th user can be written as $\gamma_k = (h_k RP_k)^2 / N_0$.

## 3 Performance analysis of the proposed NOMA scheme

In this section, the SER and ADR expressions for the proposed NOMA scheme in two-user VLC systems are derived. We assume the perfect synchronization of each symbol of U1 and U2. In addition, the input symbols are arbitrarily selected. Hence, the input symbols of U1 and U2 are equally distributed.

### 3.1 SER performance analysis

#### 3.1.1 U1's SER expression

OOK, which is a binary modulation scheme, is utilized by U1; thus, the BER is identical to the SER. For the integrity of this work, we use SER hereinafter. When bit "0" is transmitted, the sum of the sampled values follows the distribution of $f_{\mathcal{N}}(y|MRh_1P_2, M\sigma^2_{n_1})$, where $f_{\mathcal{N}}(y|\mu, \sigma^2)$ represents the Probability Density Function (PDF) of Gaussian distribution with mean $\mu$ and variance $\sigma^2$. Similarly, when bit "1" is transmitted, the sum of sampled values obeys the distribution of $f_{\mathcal{N}}(y|MRh_1(P_2 + 2P_1), M\sigma^2_{n_1})$. Given that MLD is used for U1, the corresponding threshold is the mid-point between the minimum and maximum values of the summed samples in a symbol interval, and it can be written as $\varepsilon = MRh_1(P_1 + P_2) = MRh_1P_t$. Therefore, the SER expression of U1 can be obtained as

$$\begin{aligned} P_{e_1} = &\frac{1}{2}\int_{\varepsilon}^{+\infty} f_{\mathcal{N}}(y|MRh_1P_2, M\sigma^2_{n_1})\mathrm{d}y + \\ &\frac{1}{2}\int_{-\infty}^{\varepsilon} f_{\mathcal{N}}(y|MRh_1(2P_1 + P_2), M\sigma^2_{n_1})\mathrm{d}y = \\ &\frac{1}{2}\mathrm{erfc}(\sqrt{M\gamma_1}) \end{aligned} \tag{4}$$

where erfc $(\cdot)$ is the complementary error function.

#### 3.1.2 U2's SER expression

In the proposed NOMA scheme, SDD-based $(M, N)$ MPPM is adopted by U2, which is the high bit-rate

user in the VLC system. If one symbol for U2 could be decoded correctly, the smallest value of the samples in the pulsed slots is supposed to be greater than the largest value of the samples in the unpulsed slots. Let us define three random variables $U = \max\limits_{1\leqslant i\leqslant M-N}(u_i)$, $V = \min\limits_{1\leqslant j\leqslant N}(v_j)$, and $\Phi = V - U$, where $u_i$ and $v_j$ are the sampler's output at the unpulsed and pulsed slots, respectively. If $\Phi > 0$, then U2's signal could be decoded correctly with SDD. Although the absolute optical power levels of the unpulsed slot and pulsed slot with bit "0" transmitted by U1 in the superposed signal are different from those with bit "1" transmitted, the difference of optical power level between the unpulsed slot and pulsed slot is the same regardless of U1's data. Therefore, in accordance with Ref. [44], the PDF of $\Phi$ can be obtained as Eq. (5):

$$f_{\Phi}(\varphi) = \frac{(M-N)N}{2^{M-1}\pi\sigma_{n_2}^2}\times \int_{-\infty}^{+\infty}\exp\left[-\frac{\left(\psi-\frac{MRh_2P_2}{N}\right)^2}{2\sigma_{n_2}^2}-\frac{(\varphi-\psi)^2}{2\sigma_{n_2}^2}\right]\times \left\{\operatorname{erfc}\left[\frac{\psi-\frac{MRh_2P_2}{N}}{\sqrt{2}\sigma_{n_2}}\right]\right\}^{N-1}\left\{\operatorname{erfc}\left[\frac{\varphi-\psi}{\sqrt{2}\sigma_{n_2}}\right]\right\}^{M-N-1}\mathrm{d}\psi \tag{5}$$

The SER of U2 can be further expressed as

$$P_{e_2} = \int_{-\infty}^{0} f_{\Phi}(\varphi)\,\mathrm{d}\varphi \tag{6}$$

### 3.2 ADR performance analysis

Pulse modulations are used in the proposed NOMA-VLC scheme; thus, mutual information for the $k$-th user can be expressed under the assumption of the discrete memoryless channel model as[45]

$$I_k(X_k, Y_k) = \sum_{i=1}^{\Xi_k}\sum_{j=1}^{\Xi_k} p(x_{k_i}y_{k_j})\log_2\frac{p(y_{k_j}|x_{k_i})}{p(y_{k_j})} \tag{7}$$

where $X_k = \{x_{k_1}, x_{k_2}, \ldots, x_{k_{\Xi_k}}\}$ and $Y_k = \{y_{k_1}, y_{k_2}, \ldots, y_{k_{\Xi_k}}\}$ are the sets of the transmitted and received symbols, respectively, for the $k$-th user. Both are with the size of $\Xi_k$. $p(x_{k_i}y_{k_j})$ is the joint probability that symbol $x_{k_i}$ is sent to the $k$-th user and $y_{k_j}$ is received at the receiver of the $k$-th user. It can be written as $p(x_{k_i}y_{k_j}) = p(x_{k_i})p(y_{k_j}|x_{k_i})$, where $p(x_{k_i})$ is the probability of sending $x_{k_i}$ and $p(y_{k_j}|x_{k_i})$ is the conditional probability of the event that symbol $y_{k_j}$ is received by the $k$-th user given that $x_{k_i}$ is sent. Given that the input symbols of U1 and U2 are assumed to be equally distributed, we have $p(x_{k_i}) = \frac{1}{\Xi_k}$. Furthermore, the probability distribution function of the received symbols at the $k$-th user, i.e., $p(y_{k_j})$, can be obtained as $p(y_{k_j}) = \sum\limits_{i=1}^{\Xi_k} p(x_{k_i})p(y_{k_j}|x_{k_i}) = \frac{1}{\Xi_k}\sum\limits_{i=1}^{\Xi_k} p(y_{k_j}|x_{k_i})$. From the above analysis, $I_k(X_k, Y_k)$ indicates how many bits in one symbol of the $k$-th user can convey. Let $\mathcal{R}_k$ denote the ADR of the $k$-th user. Here, we use the unit of bits per symbol, namely, bits per channel use (bpcu), to measure ADR. Therefore, we have $\mathcal{R}_k = I_k(X_k, Y_k)$.

#### 3.2.1 U1's ADR expression

OOK is a binary modulation scheme; thus, the channel between the LED and U1 can be regarded as a binary symmetric channel. Therefore, the ADR of U1 can be expressed as[45]

$$\mathcal{R}_1 = P_{e_1}\log_2(2P_{e_1}) + (1-P_{e_1})\log_2[2(1-P_{e_1})] \tag{8}$$

#### 3.2.2 U2's ADR expression

Given that U2 uses $(M, N)$ MPPM, $\Xi_2 = \mathcal{C}_M^N$, where $\mathcal{C}_M^N$ represents the number of combinations of $M$ items taken $N$ at a time. Given that $\Xi_2$ varies with the change of $M$ and $N$, the component $p(y_{2_j}|x_{2_i})$ in Eq. (7) is difficult to determine directly. However, we notice that $p(y_{2_j}|x_{2_i})$ is determined by the numbers of wrongly decoded pulsed slots or unpulsed slots in an MPPM symbol. Let us define a random variable $r = 1, \ldots, \min(N, M-N)$, which refers to the falsely decoded slots in $(M, N)$ MPPM. Based on the principle of SDD, given $r$ falsely decoded slots, $r$ pulsed slots are regarded as unpulsed slots, and $r$ unpulsed slots are considered as pulsed slots. We further define three random variables $U' = \max\{u_1, \ldots, u_{M-N-r}, v_{N-r+1}, \ldots, v_N\}$, $V' = \min\{v_1, \ldots, v_{N-r}, u_{M-N-r+1}, \ldots, u_{M-N}\}$, and $\Phi' = V' - U'$, where $u_i$ $(i = 1, \ldots, M-N)$ denotes the sampled values of the slots that should be unpulsed, and $v_j$ $(j = 1, \ldots, N)$ represents the sampled values of the slots that should be pulsed. In the set of sampled values $\{u_1, \ldots, u_{M-N-r}, v_{N-r+1}, \ldots, v_N\}$, it contains $r$ wrongly decoded unpulsed slots that

should be pulsed. Similarly, the set of sampled values $\{v_1, \ldots, v_{N-r}, u_{M-N-r+1}, \ldots, u_{M-N}\}$ includes $r$ wrongly decoded pulsed slots.

**Theorem 1** The probability of $r$ can be written as

$$p_r(r) = \int_0^{+\infty} f_{\Phi'}(\varphi)\, \mathrm{d}\varphi \tag{9}$$

where $f_{\Phi'}(\varphi)$ is the PDF of $\Phi'$ and can be obtained as Eq. (10):

$$\begin{aligned} f_{\Phi'}(\varphi) = & \int_{-\infty}^{+\infty} \left\{ \frac{N-r}{\sqrt{2\pi}\sigma_{n_2}} \exp\left[ -\frac{\left(\varphi-\psi-\frac{MRh_2P_2}{N}\right)^2}{2\sigma_{n_2}^2} \right] \times \right. \\ & \left[ \frac{1}{2}\mathrm{erfc}\left( \frac{\varphi-\psi-\frac{MRh_2P_2}{N}}{\sqrt{2}\sigma_{n_2}} \right) \right]^{N-r-1} \left[ \frac{1}{2}\mathrm{erfc}\left( \frac{\varphi-\psi}{\sqrt{2}\sigma_{n_2}} \right) \right]^{r} + \\ & \frac{r}{\sqrt{2\pi}\sigma_{n_2}} \exp\left( -\frac{(\varphi-\psi)^2}{2\sigma_{n_2}^2} \right) \left[ \frac{1}{2}\mathrm{erfc}\left( \frac{\varphi-\psi-\frac{MRh_2P_2}{N}}{\sqrt{2}\sigma_{n_2}} \right) \right]^{N-r} \times \\ & \left. \left[ \frac{1}{2}\mathrm{erfc}\left( \frac{\varphi-\psi}{\sqrt{2}\sigma_{n_2}} \right) \right]^{r-1} \right\} \left\{ \frac{M-N-r}{\sqrt{2\pi}\sigma_{n_2}} \exp\left( -\frac{\psi^2}{2\sigma_{n_2}^2} \right) \times \right. \\ & \left[ \frac{1}{2}\mathrm{erfc}\left( \frac{\psi}{\sqrt{2}\sigma_{n_2}} \right) \right]^{M-N-r-1} \left[ \frac{1}{2}\mathrm{erfc}\left( \frac{\frac{MRh_2P_2}{N}+\psi}{\sqrt{2}\sigma_{n_2}} \right) \right]^{r} + \\ & \frac{r}{\sqrt{2\pi}\sigma_{n_2}} \exp\left[ -\frac{\left(-\psi-\frac{MRh_2P_2}{N}\right)^2}{2\sigma_{n_2}^2} \right] \times \\ & \left. \left[ \frac{1}{2}\mathrm{erfc}\left( \frac{\psi}{\sqrt{2}\sigma_{n_2}} \right) \right]^{M-N-r} \left[ \frac{1}{2}\mathrm{erfc}\left( \frac{\frac{MRh_2P_2}{N}+\psi}{\sqrt{2}\sigma_{n_2}} \right) \right]^{r-1} \right\} \mathrm{d}\psi \end{aligned} \tag{10}$$

**Proof** Given that SDD only concerns the relationship among optical power levels of the pulsed and unpulsed slots, it has no effect on the decoding results of U2' signals that U1 sends bit "0" or "1" because during an MPPM symbol interval, U1's signal remains at a constant power level. Here, we prove Theorem 1 with the assumption that U1 sends bit "0". The same results can be achieved when U1 sends bit "1".

Random variable $u_i$ obeys the distribution of $f_{\mathcal{N}}\left(u \,|0, \sigma_{n_2}^2\right)$. Its Cumulative Distribution Function (CDF) can be written as

$$F_{u_i}(u) = \frac{1}{2}\mathrm{erfc}\left( -\frac{u}{\sqrt{2}\sigma_{n_2}} \right) \tag{11}$$

In addition, random variable $v_j$ follows the distribution of $f_{\mathcal{N}}\left(v \,\middle|\, \frac{MRh_2P_2}{N}, \sigma_{n_2}^2\right)$. Its CDF can be expressed as

$$F_{v_j}(v) = \frac{1}{2}\mathrm{erfc}\left( \frac{\frac{MRh_2P_2}{N}-v}{\sqrt{2}\sigma_{n_2}} \right) \tag{12}$$

In accordance with Eqs. (6-55), (6-57), and (6-58) in Ref. [46], the CDFs of $U'$ and $V'$ can be obtained as

$$F_{U'}(u) = F_{u_i}(u)^{M-N-r} F_{v_j}(u)^r \tag{13}$$

and

$$F_{V'}(v) = 1 - \left[1 - F_{v_j}(v)\right]^{N-r} \left[1 - F_{u_i}(v)\right]^r \tag{14}$$

respectively. Furthermore, by differentiating Eq. (13) with respect to $u$ and Eq. (14) with respect to $v$, the PDFs of $U'$ and $V'$ can be derived as Eqs. (15) and (16), respectively.

$$\begin{aligned} f_{U'}(u) = & \frac{M-N-r}{\sqrt{2\pi}\sigma_{n_2}} \exp\left( -\frac{u^2}{2\sigma_{n_2}} \right) \times \\ & \left[ \frac{1}{2}\mathrm{erfc}\left( -\frac{u}{\sqrt{2}\sigma_{n_2}} \right) \right]^{M-N-r-1} \left[ \frac{1}{2}\mathrm{erfc}\left( \frac{\frac{MRh_2P_2}{N}-u}{\sqrt{2}\sigma_{n_2}} \right) \right]^{r} + \\ & \frac{r}{\sqrt{2\pi}\sigma_{n_2}} \exp\left[ -\frac{\left(u-\frac{MRh_2P_2}{N}\right)^2}{2\sigma_{n_2}^2} \right] \times \\ & \left[ \frac{1}{2}\mathrm{erfc}\left( -\frac{u}{\sqrt{2}\sigma_{n_2}} \right) \right]^{M-N-r} \left[ \frac{1}{2}\mathrm{erfc}\left( \frac{\frac{MRh_2P_2}{N}-u}{\sqrt{2}\sigma_{n_2}} \right) \right]^{r-1} \end{aligned} \tag{15}$$

$$\begin{aligned} f_{V'}(v) = & \frac{N-r}{\sqrt{2\pi}\sigma_{n_2}} \exp\left[ -\frac{\left(v-\frac{MRh_2P_2}{N}\right)^2}{2\sigma_{n_2}^2} \right] \times \\ & \left[ \frac{1}{2}\mathrm{erfc}\left( \frac{v-\frac{MRh_2P_2}{N}}{\sqrt{2}\sigma_{n_2}} \right) \right]^{N-r-1} \left[ \frac{1}{2}\mathrm{erfc}\left( \frac{v}{\sqrt{2}\sigma_{n_2}} \right) \right]^{r} + \\ & \frac{r}{\sqrt{2\pi}\sigma_{n_2}} \exp\left( -\frac{v^2}{2\sigma_{n_2}^2} \right) \left[ \frac{1}{2}\mathrm{erfc}\left( \frac{v-\frac{MRh_2P_2}{N}}{\sqrt{2}\sigma_{n_2}} \right) \right]^{N-r} \times \\ & \left[ \frac{1}{2}\mathrm{erfc}\left( \frac{v}{\sqrt{2}\sigma_{n_2}} \right) \right]^{r-1} \end{aligned} \tag{16}$$

Then the PDF of $\Phi'$ can be expressed as

$$f_{\Phi'}(\varphi) = f_{V'}(\varphi) * f_{-U'}(\varphi) = f_{V'}(\varphi) * f_{U'}(-\varphi) \tag{17}$$

where $*$ denotes the convolution operator. By substituting Eqs. (15) and (16) into Eq. (17), we can obtain Eq. (10). If there are $r$ incorrectly received pulsed or unpulsed slots, then $\Phi' > 0$ should be satisfied. Lastly, Eq. (9) can be obtained by integrating Eq. (10) from 0 to positive infinite. ■

The correctness of Theorem 1 is also verified by MC simulation, which is given in the Appendix. In addition,

the expressions of asymptotic approximation in low and high SNR regions for Eq. (9) are provided to facilitate the numerical calculation.

With the help of Eq. (9), $p(y_{2_j}|x_{2_i})$ could be easily calculated by counting how many slots are wrongly decoded. Therefore, we can obtain $p(y_{2_j})$ as follows:

$$p(y_{2_j}) = \frac{1}{\Xi_2}\sum_{i=1}^{\Xi_2} p(y_{2_j}|x_{2_i}) = \frac{1}{\mathcal{C}_M^N}\left[(1-P_{e_2}) + \sum_{r=1}^{\min(N,M-N)} \mathcal{C}_N^r \mathcal{C}_{M-N}^r p_r(r)\right] \tag{18}$$

By substituting Eq. (18) into Eq. (7), the ADR of U2 can be derived as follows:

$$\mathcal{R}_2 = (1-P_{e_2})\log_2\frac{(1-P_{e_2})}{p(y_{2_j})} + \sum_{r=1}^{\min(N,M-N)} \mathcal{C}_N^r \mathcal{C}_{M-N}^r p_r(r)\log_2\frac{p_r(r)}{p(y_{2_j})} \tag{19}$$

### 3.2.3 Sum rate of the proposed NOMA scheme

On the basis of Eqs. (8) and (19), the sum rate of the proposed NOMA scheme in the two-user VLC systems can be written as

$$\mathcal{R}_\mathrm{s} = \sum_{k=1}^{2} \mathcal{R}_k \tag{20}$$

To compare with the conventional OMA scheme, the sum rate expression of the conventional OMA scheme in the two-user VLC system is also given as follows:

$$\mathcal{R}_\mathrm{s}^\mathrm{OMA} = \sum_{k=1}^{2} \beta_k \mathcal{R}_k \tag{21}$$

where $\beta_k$ is the orthogonal resource allocation factor, ranging from 0 to 1.

## 4 Result and discussion

In this section, the SER and ADR results of the proposed NOMA scheme in a two-user VLC system, which consists of a single LED and two users, are analyzed and discussed. The LED is mounted on the center of the ceiling of a room with a size of 4 m × 4 m × 3 m. Under the assumption that U2 is closer to the LED than U1, U2 could achieve better channel quality than U1. Without loss of generality, let U1 be at the location with the coordinates of (2 m, 1.5 m, 1.25 m) and U2 be at the location with the coordinates of (1.8 m, 2 m, 1.25 m). Other parameters, which are related to VLC channel and used in the process of analytical calculation and MC simulation, are given in Table 1 unless otherwise specified. Therefore, the channel gains of U1 ($h_1$) and U2 ($h_2$) are equal to $1.7088 \times 10^{-4}$ and $1.9480 \times 10^{-4}$, respectively. Unless otherwise stated, U2 adopts (5, 2) MPPM. Considering that different users' signals encounter different channel gains, the SER and ADR performances of different users are evaluated with the same transmitting SNR $\gamma$ to provide a fair comparison[34,35]. The relationship between transmitting SNR and the average electrical SNR at the $k$-th user can be expressed as $\gamma_1 = h_1^2\alpha^2\gamma^2$ and $\gamma_2 = h_2^2(1-\alpha)^2\gamma^2$. During MC simulation, a total of $5 \times 10^7$ symbols for U1 and U2 are generated to reduce the uncertainties of the SER. We still use Eq. (9) to calculate the ADR results of U2 in this section because of its accuracy.

The SER performance of the proposed NOMA scheme in two-user VLC systems with regard to transmitting

**Table 1 Used parameters.**

| Parameter name | Notation | Value |
|---|---|---|
| LED semi-angle | $\psi_{1/2}$ (°) | 60 |
| PD HFOV | $\varphi_\mathrm{c}$ (°) | 45 |
| PD detection area | $A_k$ (cm$^2$) | 1 |
| PD responsivity | $R$ (A/W) | 1 |
| Optical filter gain | $T(\varphi_k)$ | 1 |
| Reflective index of optical concentrator | $\rho$ | 1.5 |

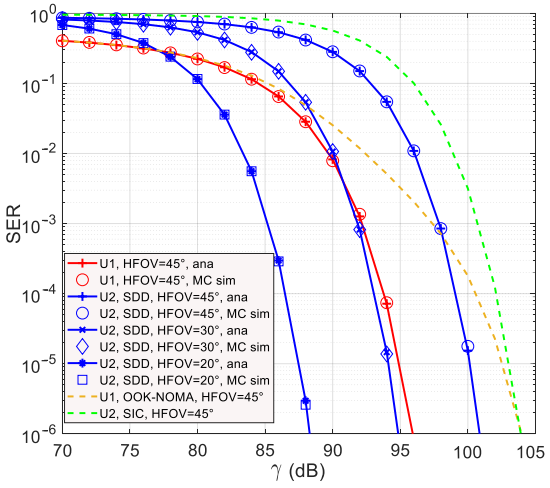


**Fig. 3 SER performance of two-user NOMA-VLC systems with OOK and SDD-based MPPM. The results of U2 with SIC-based MPPM and U1 in the variable rate OOK-based NOMA system[39] are also plotted here for comparison.**

SNR is demonstrated in Fig. 3. Different HFOVs ($\varphi_c = 45°$, 30°, and 20°), which are adopted by U2, are considered. The power allocation factor is set to be 0.6, i.e., $\alpha = 0.6$. Given that the channel gains of each user are in the order of $10^{-4}$, a 70 dB offset of transmitting SNR is provided to depict the analytical and simulation results clearly. The analytical results ("ana" for short in the legend of Fig. 3) have perfect agreements with MC simulation ("sim" for short) results, confirming the correctness of our theoretical SER expressions. In addition, although low optical power is allocated to U2, using the PD with narrow HFOV could achieve improved SER performance. For example, when $\gamma$ equals 88 dB, the SER values of U2 are roughly $4 \times 10^{-1}$, $5 \times 10^{-2}$, and $3 \times 10^{-6}$ for $\varphi_c = 45°, 30°$, and 20°, respectively, because narrower HFOV will contribute to better channel gain in accordance with Formula (1). Furthermore, the SER results of U1, namely, the low bit-rate user, in the variable-rate OOK-based NOMA scheme[39] with a bit-rate factor set to 5 and two users are given here for comparison, which is abbreviated to "OOK-NOMA" in the legend and obtained via MC simulation. When MPPM is used by U2, the SER performance of U1 is better, especially when the transmitting SNR increases, because MPPM has constant power in each symbol interval compared with the random signal power of the high bit-rate user in the variable-rate OOK-based NOMA scheme. Furthermore, the results of the SIC-based MPPM decoding scheme with MLD are depicted for comparison (abbreviated as "SIC" in the legend) and obtained through MC simulation. The SER performance of U2 with SDD-based MPPM is better than that with SIC-based MPPM. This result is obtained because exploiting the relative optical power levels among the slots within an MPPM block, which is different from the SIC scheme with MLD where the absolute optical power levels are used, plays a vital role in performing the SDD and achieving better SER performance.

In Fig. 4, the SER performance of the proposed NOMA scheme in two-user VLC systems with different power allocation factors is plotted. To compare the SER performance of U1 and U2 fairly, we assume that these two users are at the same location. Hence, they have the same channel gain. For simplicity, let

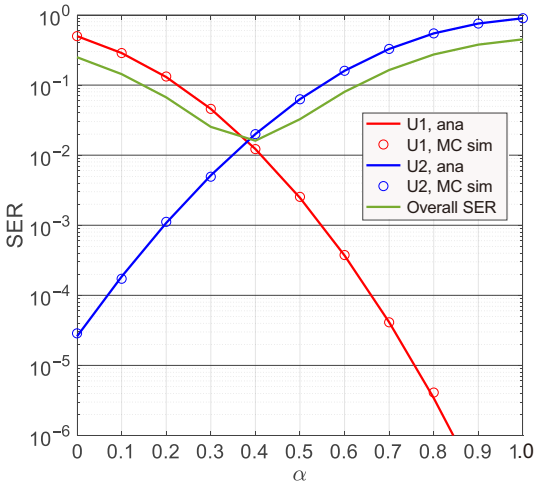


**Fig. 4 SER performance of two-user NOMA-VLC systems with different power allocation factors considered.**

it be unity in Fig. 4. The transmitting SNR is set to 5 dB, i.e., $\gamma = 5$ dB. Even though U1 is under poor SER performance condition, it exerts no influence on U2's SER performance. That is, no EP exists anymore. This result is obtained because SDD-based MPPM is adopted here and SIC is not required. Hence, the EP is totally eliminated. The curve of the overall SER is also given in Fig. 4. The overall SER is defined as $P_e = 0.5P_{e_1} + 0.5P_{e_2}$ because the symbol rates of OOK and MPPM are assumed to be the same, and all symbols are synchronized. The optimal overall SER can be achieved when the power allocation factor is around the intersection of the curves of U1 and U2.

Figure 5 demonstrates the ADR performance of the proposed NOMA scheme in two-user VLC systems versus the power allocation factors with four different transmitting SNR values considered, including $\gamma = 85$, 90, 95, and 100 dB. As shown in Fig. 5, when $\gamma$ is equal to 85 dB, the sum rate of the NOMA-VLC system decreases as $\alpha$ increases. However, when $\gamma$ is equal to 90, 95, and 100 dB, the curves of the sum rate increase first and then decrease after reaching their maximum values. Especially for $\gamma = 100$ dB, there is a wide region of $\alpha$, roughly from 0.3 to 0.6, that sum rate remains the maximum value of the considered NOMA-VLC system, which is denoted as $\mathcal{R}_s^{\max}$ in Fig. 5 and equals $\log_2(\Xi_1\Xi_2) = \log_2\left(2 \times C_5^2\right) \approx 4.32$ bpcu. This result is obtained because the ADR of the high bit-rate user contributes more to the sum rate in the

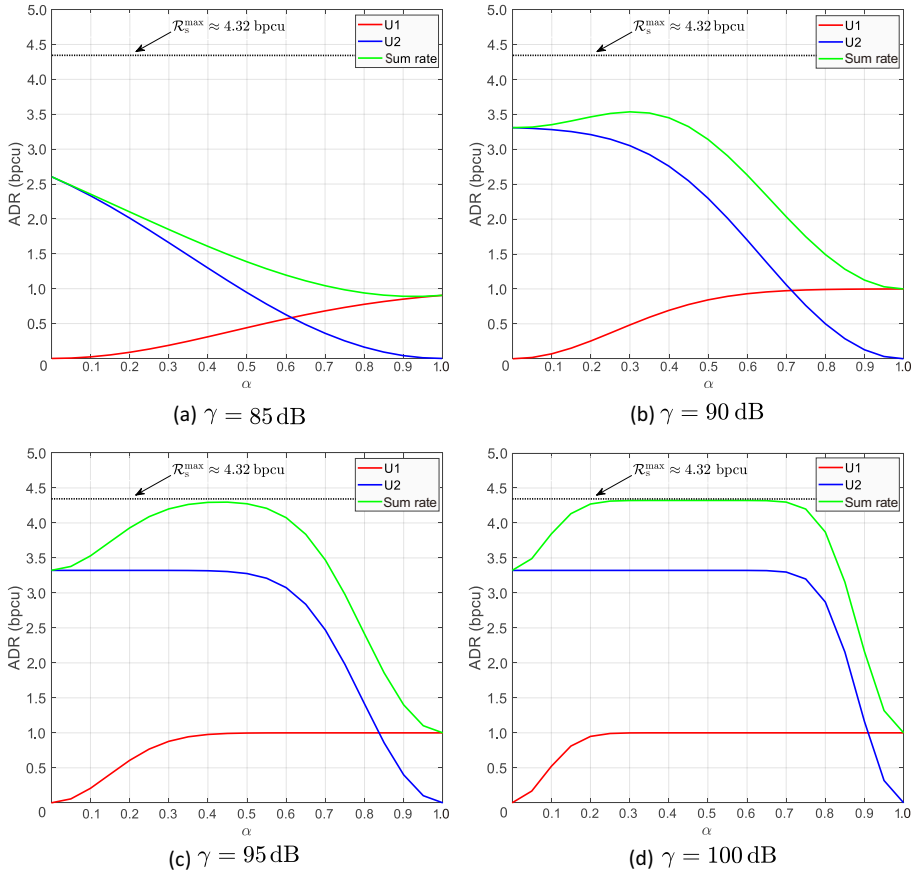


**Fig. 5 ADR performance of two-user NOMA-VLC systems versus power allocation factors when transmitting SNR equals (a) 85, (b) 90, (c) 95, and (d) 100 dB.**

considered system compared with that of the low bit-rate user. $\gamma = 85$ dB represents a poor VLC channel condition. At this time, U2 cannot reach its maximum ADR, which equals $\log_2(\Xi_2) \approx 3.32$ bpcu, even though all the transmitting power are allocated to it, i.e., $\alpha = 0$. Nevertheless, with the increase in $\gamma$, this situation could be relived because a high transmitting SNR allows U2 to reach its maximum ADR even with less power allocated. Additional rest power could be assigned to U1, thus giving U1 the chance to reach its maximum ADR. In Figs. 6 and 7, we adopt $\alpha = 0.45$ because it is the medium point of the region that sum rate could achieve the maximum value at $\gamma = 100$ dB.

In Fig. 6, we compare the ADR performance of the proposed NOMA scheme with that of conventional OMA scheme. Without loss of generality, the orthogonal resource allocation factor is set to 0.5 ($\beta_k = 0.5$) for two users in the OMA scheme, indicating that these two users have an equal chance to utilize the orthogonal resources. In addition, we assume that the users in the

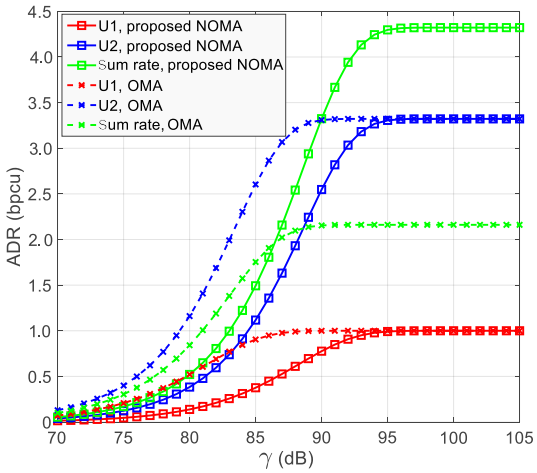


**Fig. 6 Comparison of ADR between the proposed NOMA scheme and the conventional OMA scheme, in which we set $\beta_k = 0.5$.**

OMA scheme could be allocated with full transmission power when they obtain the chance to use the channel. As shown in Fig. 6, the maximum ADR results of the NOMA and OMA schemes are the same for U1 and U2. That is, the maximum ADR of U1 is 1.0 bpcu, and that of

U2 is approximately 3.32 bpcu for the NOMA and OMA schemes. This result is obtained because the ADR results are determined by the adopted modulation schemes, and the same modulation schemes are used in NOMA and OMA. In addition, U1 and U2 in the OMA scheme could reach their maximum values at lower SNR conditions because full transmission power is assigned to the user who uses the channel. However, the maximum sum rate of the proposed NOMA scheme is approximately 4.32 bpcu, which is higher than that of the OMA scheme (i.e., approximately 2.16 bpcu). This result is obtained because two users in the NOMA scheme could utilize the orthogonal resources of the VLC channel all the time, whereas those in the OMA scheme can only use the orthogonal resources when they get the chance, which is controlled by $\beta_k$. Therefore, the proposed NOMA scheme could facilitate the improvement of the system-level throughput.

The effect of different numbers of total slots $M$ and pulsed slots $N$ in one MPPM symbol adopted by the high bit-rate user on the ADR performance of the proposed NOMA scheme is illustrated in Figs. 7a and 7b, respectively. In Fig. 7a, we fix $N = 2$ and set $M = 4$, 5, and 6. The ADR of U1 increases as $M$ increases at the same transmitting SNR in the rising stage because the larger the number of slots in one MPPM, the more sampled values are brought for U1 to sum, thus effectively reducing the fluctuation of the signal power of U1 caused by noise. Therefore, the quality of U1's signal could be enhanced. In addition, the maximum ADR of U2 is boosted by increasing $M$. Hence, the higher sum rate could be achieved as $M$ increases. This result is obtained because the results of combination $\Xi_2 = \mathcal{C}_M^N$ become larger when $N$ is fixed and $M$ increases. For example, the maximum ADRs of U2 are roughly 2.59, 3.32, and 3.91 bpcu for $(4, 2)$ MPPM, $(5, 2)$ MPPM, and $(6, 2)$ MPPM, respectively. In Fig. 7b, we fix $M = 6$ and set $N = 1$, 3, and 5. The ADR results of U1 are identical under all conditions because $M$ is the same. Moreover, the maximum ADR of U2 with $(6, 3)$ MPPM is higher than that of the other two scenarios because $\mathcal{C}_6^3 \approx 4.32 > \mathcal{C}_6^1 = \mathcal{C}_6^5 \approx 2.58$. The rising stage of the ADR of U2 with $(6, 1)$ MPPM happens earlier than that with $(6, 5)$ MPPM as $\gamma$ increases. Compared with $(6, 5)$

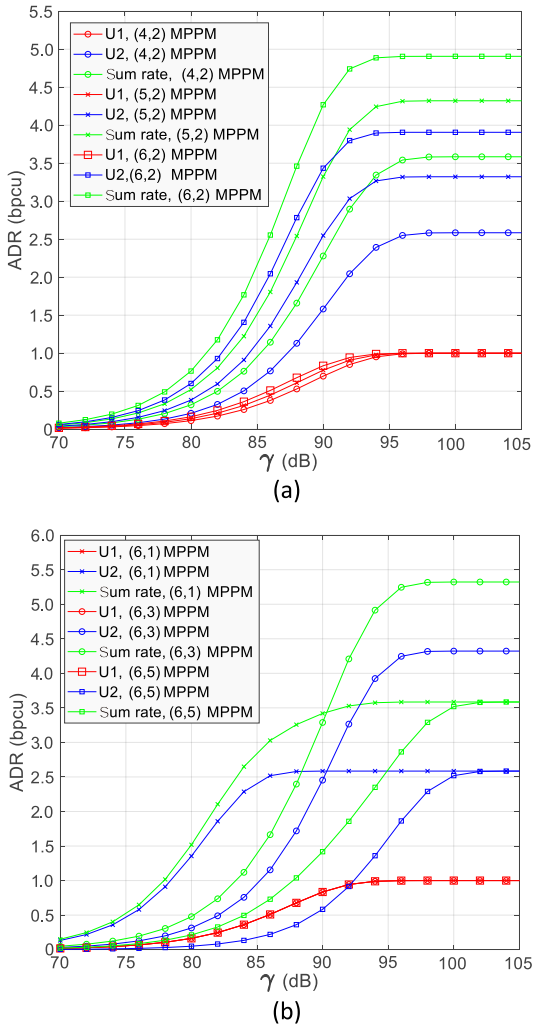


**Fig. 7 ADR versus transmitting SNR with different numbers of (a) total slots and (b) pulsed slots adopted by the high bit-rate user.**

MPPM, $(6, 1)$ MPPM could offer more SNR gains to reach the same ADR. For instance, to achieve the ADR of 2 bpcu, $(6, 1)$ MPPM has approximately 14 dB SNR gain than $(6, 5)$ MPPM because under the same average transmission power constraint, the difference of power level between the pulsed and unpulsed slots of $(6, 1)$ MPPM is larger than that of $(6, 5)$ MPPM, which helps the decoder of U2 to make correct decisions. That is, if the same maximum ADR of the high bit-rate user could be achieved, a small $N$ could be beneficial under low transmitting SNR conditions.

## 5 Conclusion

In this study, a novel downlink NOMA scheme, which could serve users with different requirements of data

rate, in VLC systems with different pulse modulations was proposed. The low bit-rate user adopted OOK modulation, and the high bit-rate user used SDD-based MPPM. The expressions for SER and ADR performance were derived. MC simulation results were also provided to verify the correctness of the theoretical results. Results demonstrated that the proposed NOMA scheme could fundamentally eliminate the effect of EP because SDD-based MPPM was adopted by the high bit-rate user. Furthermore, the proposed NOMA scheme could achieve a better sum rate of system than conventional OMA schemes. Increasing the values of combination $\mathcal{C}_M^N$ could boost the maximum ADR of the high bit-rate user. When the total slots in one MPPM symbol are the same, the smaller $N$ could provide more SNR gains if the maximum ADR of the high bit-rate users is the same. In practical VLC systems, all users can be divided into two groups based on the required data transmission rate. One group with low data rate requirement utilizes the OOK modulation, and the other uses the MPPM scheme. For this scenario, Time Division Multiple Access (TDMA) or other OMA schemes could be exploited within each group to increase connectivity. Considering that the MPPM and OOK modulation schemes are suitable for dimming control[41], we will investigate our proposed NOMA scheme in VLC systems with dimming control strategy in the future.

## Appendix

In this part, the expressions of asymptotic approximation in low and high SNR regions for the probability of $r$, i.e., $p_r(r)$, are obtained.

When the proposed NOMA-VLC system works under low SNR conditions, the decoder of the high bit-rate user is similar to choosing a symbol randomly from the set that contains $\Xi_2$ possible options. Therefore, when SNR is low, the $p_r(r)$ can be approximately expressed as

$$p_r^L(r) = \frac{1}{\Xi_2} = \frac{1}{\mathcal{C}_M^N} \tag{A1}$$

When high SNR scenarios are considered, the random variables $U'$ and $V'$ can be approximately expressed as $U' \approx \max\{v_{N-r+1}, \ldots, v_N\}$, $V' \approx \min\{u_{M-N-r+1}, \ldots, u_{M-N}\}$. To obtain the PDF of $U'$ and $V'$ under high SNR conditions, we further define three equivalent random variables $U'' = \max_{1\leqslant j\leqslant r}(v_j)$, $V'' = \min_{1\leqslant i\leqslant r}(u_i)$, and $\Phi'' = V'' - U''$. After similar manipulations in the proof of Theorem 1 , the PDF of $U''$ and $V''$ can be expressed as

$$f_{U''}(u) = \frac{r}{\sqrt{2\pi}\sigma_{n_2}} \exp\left[-\frac{\left(u - \frac{MRh_2P_2}{N}\right)^2}{2\sigma_{n_2}^2}\right] \times \left[\frac{1}{2}\mathrm{erfc}\left(\frac{\frac{MRh_2P_2}{N} - u}{\sqrt{2}\sigma_{n_2}}\right)\right]^{r-1} \tag{A2}$$

and

$$f_{V''}(v) = \frac{r}{\sqrt{2\pi}\sigma_{n_2}} \exp\left(-\frac{v^2}{2\sigma_n^2}\right)\left[\frac{1}{2}\mathrm{erfc}\left(\frac{v}{\sqrt{2}\sigma_{n_2}}\right)\right]^{r-1} \tag{A3}$$

respectively. The PDF of $\Phi''$ can be further obtained as

$$f_{\Phi''}(\varphi) = \frac{r^2}{2^{2r-1}\pi\sigma_{n_2}^2} \times \int_{-\infty}^{+\infty} \exp\left[-\frac{(\varphi-\psi)^2 + \left(-\psi - \frac{MRh_2P_2}{N}\right)^2}{2\sigma_{n_2}^2}\right] \times \left[\mathrm{erfc}\left(\frac{\frac{MRh_2P_2}{N} + \psi}{\sqrt{2}\sigma_{n_2}}\right)\mathrm{erfc}\left(\frac{\varphi-\psi}{\sqrt{2}\sigma_{n_2}}\right)\right]^{r-1} \mathrm{d}\psi \tag{A4}$$

Hence, when the system works under high SNR conditions, $p_r(r)$ can be approximately written as

$$p_r^H(r) = \int_0^{+\infty} f_{\Phi''}(\varphi)\,\mathrm{d}\varphi \tag{A5}$$

In Fig. A1, the curve of $p_r(r)$ is plotted versus transmitting SNR. The adopted parameters are identical

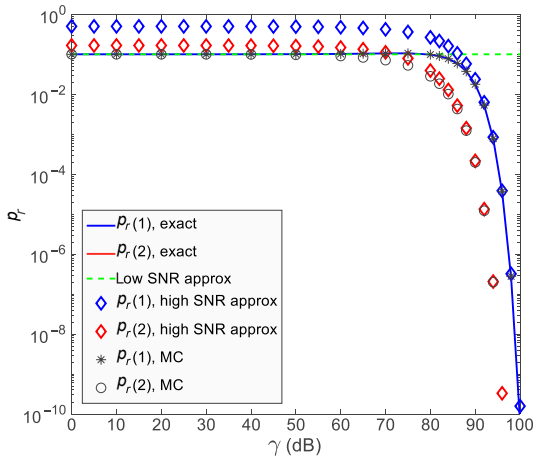


**Fig. A1 Curve of the probability of the number of wrongly decoded pulsed or unpulsed slots for the high bit-rate user (U2) with (5, 2) MPPM adopted with regard to transmitting SNR.**

to those used in Section 4. Given that $(5, 2)$ MPPM is used by U2, $r$ could be 1 or 2. In Fig. A1, the exact results of $p_r(r)$ are obtained via Eq. (9) and demonstrated with solid lines, where the blue line is for $r = 1$ and the red line is for $r = 2$. "Low SNR approx" in the legend denotes the asymptotically approximated results under the low SNR region obtained from Eq. (A1). Similarly, "high SNR approx" represents the asymptotically approximated results under the high SNR region obtained from Eq. (A5). MC results are given as discrete markers, which are obtained with $10^8$ random tests. As shown in Fig. A1, the exact results have excellent agreement with the MC results, thus verifying the correctness of Eq. (9). Furthermore, the asymptotic results of $p_r(r)$ under low and high SNR regions can tightly approximate the exact ones.

**Acknowledgment**

This work was supported by the National Key Research and Development Program of China (No. 2017YFB0403403) and the Natural Science Foundation of Guangdong Province (No. 2015A030312006).

## References

[1] D. Karunatilaka, F. Zafar, V. Kalavally, and R. Parthiban, LED based indoor visible light communications: State of the art, *IEEE Commun. Surveys Tutor.*, vol. 17, no. 3, pp. 1649–1678, 2015.

[2] J. Y. Sung, C. W. Chow, and C. H. Yeh, Dimming-discrete-multi-tone (DMT) for simultaneous color control and high speed visible light communication, *Opt. Express*, vol. 22, no. 7, pp. 7538–7543, 2014.

[3] J. Song, W. B. Ding, F. Yang, H. Yang, B. Y. Yu, and H. M. Zhang, An indoor broadband broadcasting system based on PLC and VLC, *IEEE Trans. Broadcast.*, vol. 61, no. 2, pp. 299–308, 2015.

[4] B. Y. Yu, H. M. Zhang, L. Wei, and J. Song, Subcarrier grouping OFDM for visible-light communication systems, *IEEE Photon. J.*, vol. 7, no. 5, p. 7903812, 2015.

[5] X. Huang, F. Yang, C. Y. Pan, and J. Song, Advanced ADO-OFDM with adaptive subcarrier assignment and optimized power allocation, *IEEE Wirel. Commun. Lett.*, vol. 8, no. 4, pp. 1167–1170, 2019.

[6] S. Z. Chen, Y. C. Liang, S. H. Sun, S. L. Kang, W. C. Cheng, and M. G. Peng, Vision, requirements, and technology trend of 6G: How to tackle the challenges of system coverage, capacity, user data-rate and movement speed, *IEEE Wirel. Commun.*, vol. 27, no. 2, pp. 218–228, 2020.

[7] M. Giordani, M. Polese, M. Mezzavilla, S. Rangan, and M. Zorzi, Toward 6G networks: Use cases and technologies, *IEEE Commun. Mag.*, vol. 58, no. 3, pp. 55–61, 2020.

[8] H. L. Minh, D. O'Brien, G. Faulkner, L. B. Zeng, K. Lee, D. Jung, Y. Oh, and E. T. Won, 100-Mb/s NRZ visible light communications using a postequalized white LED, *IEEE Photon. Technol. Lett.*, vol. 21, no. 15, pp. 1063–1065, 2009.

[9] L. B. Zeng, D. C. O'Brien, H. Le Minh, G. E. Faulkner, K. Lee, D. Jung, Y. Oh, and E. T. Won, High data rate multiple input multiple output (MIMO) optical wireless communications using white LED lighting, *IEEE J. Selected Areas Commun.*, vol. 27, no. 9, pp. 1654–1662, 2009.

[10] S. M. Feng, R. Zhang, W. Xu, and L. Hanzo, Multiple access design for ultra-dense VLC networks: Orthogonal vs non-orthogonal, *IEEE Trans. Commun.*, vol. 67, no. 3, pp. 2218–2232, 2019.

[11] L. L. Dai, B. C. Wang, Z. G. Ding, Z. C. Wang, S. Chen, and L. Hanzo, A survey of non-orthogonal multiple access for 5G, *IEEE Commun. Surveys Tutor.*, vol. 20, no. 3, pp. 2294–2323, 2018.

[12] R. Hoshyar, F. P. Wathan, and R. Tafazolli, Novel low-density signature for synchronous CDMA systems over AWGN channel, *IEEE Trans. Signal Proc.*, vol. 56, no. 4, pp. 1616–1626, 2008.

[13] H. Marshoud, S. Muhaidat, P. C. Sofotasios, S. Hussain, M. Ali Imran, and B. S. Sharif, Optical non-orthogonal multiple access for visible light communication, *IEEE Wirel. Commun.*, vol. 25, no. 2, pp. 82–88, 2018.

[14] H. R. Wang, F. S. Wang, and R. Li, Enhancing power allocation efficiency of NOMA aided-MIMO downlink VLC networks, *Opt. Commun.*, vol. 454, p. 124497, 2020.

[15] H. Marshoud, V. M. Kapinas, G. K. Karagiannidis, and S. Muhaidat, Non-orthogonal multiple access for visible light communications, *IEEE Photon. Technol. Lett.*, vol. 28, no. 1, pp. 51–54, 2016.

[16] C. Chen, W. D. Zhong, H. L. Yang, and P. F. Du, On the performance of MIMO-NOMA-based visible light communication systems, *IEEE Photon. Technol. Lett.*, vol. 30, no. 4, pp. 307–310, 2018.

[17] Z. H. Yang, W. Xu, and Y. R. Li, Fair non-orthogonal multiple access for visible light communication downlinks, *IEEE Wirel. Commun. Lett.*, vol. 6, no. 1, pp. 66–69, 2017.

[18] Y. Fu, Y. Hong, L. K. Chen, and C. W. Sung, Enhanced power allocation for sum rate maximization in OFDM-NOMA VLC systems, *IEEE Photon. Technol. Lett.*, vol. 30, no. 13, pp. 1218–1221, 2018.

[19] Q. Li, T. Shang, T. Tang, and Z. Y. Dong, Optimal power allocation scheme based on multi-factor control in indoor NOMA-VLC systems, *IEEE Acc.*, vol. 7, pp. 82 878–82 887, 2019.

[20] S. M. Feng, T. Bai, and L. Hanzo, Joint power allocation for the multi-user NOMA-downlink in a power-line-fed VLC network, *IEEE Trans. Vehicul. Technol.*, vol. 68, no. 5, pp. 5185–5190, 2019.

[21] B. J. Lin, W. P. Ye, X. Tang, and Z. Ghassemlooy, Experimental demonstration of bidirectional NOMA-OFDMA visible light communications, *Opt. Express*, vol. 25, no. 4, pp. 4348–4355, 2017.

[22] H. Abumarshoud, H. Alshaer, and H. Haas, Dynamic multiple access configuration in intelligent lifi attocellular access points, *IEEE Acc.*, vol. 7, pp. 62 126–62 141, 2019.

[23] L. Yin, W. O. Popoola, X. P. Wu, and H. Haas, Performance evaluation of non-orthogonal multiple access in visible light communication, *IEEE Trans. Commun.*, vol. 64, no. 12, pp. 5162–5175, 2016.

[24] M. B. Janjua, D. B. Da Costa, and H. Arslan, User pairing and power allocation strategies for 3D VLC-NOMA systems, *IEEE Wirel. Commun. Lett.*, vol. 9, no. 6, pp. 866–870, 2020.

[25] G. Nauryzbayev, M. Abdallah, and H. Elgala, On the performance of NOMA-enabled spectrally and energy efficient OFDM (SEE-OFDM) for indoor visible light communications, in *Proc. 2018 IEEE* $87^{th}$ *Vehicular Technology Conf.* (*VTC Spring*), Porto, Portugal, 2018.

[26] G. Nauryzbayev, M. Abdallah, and H. Elgala, Outage of SEE-OFDM VLC-NOMA networks, *IEEE Photon. Technol. Lett.*, vol. 31, no. 2, pp. 121–124, 2019.

[27] H. Y. Li, Z. T. Huang, Y. Xiao, S. Zhan, and Y. F. Ji, A power and spectrum efficient NOMA scheme for VLC network based on hierarchical pre-distorted LACO-OFDM, *IEEE Acc.*, vol. 7, pp. 48 565–48 571, 2019.

[28] J. Shi, J. He, K. Q. Wu, and J. Ma, Enhanced performance of asynchronous multi-cell VLC system using OQAM/OFDM-NOMA, *J. Lightw. Technol.*, vol. 37, no. 20, pp. 5212–5220, 2019.

[29] A. Adnan, Y. Liu, C. W. Chow, and C. H. Yeh, Demonstration of non-hermitian symmetry (NHS) IFFT/FFT size efficient OFDM non-orthogonal multiple access (NOMA) for visible light communication, *IEEE Photon. J.*, vol. 12, no. 3, p. 7201405, 2020.

[30] A. Adnan, Y. Liu, C. W. Chow, and C. H. Yeh, Analysis of non-hermitian symmetry (NHS) IFFT/FFT size efficient OFDM for multiple-client non-orthogonal multiple access (NOMA) visible light communication (VLC) system, *Opt. Commun.*, vol. 472, p. 125991, 2020.

[31] X. Zhao, H. B. Chen, and J. Y. Sun, On physical-layer security in multiuser visible light communication systems with non-orthogonal multiple access, *IEEE Acc.*, vol. 6, pp. 34 004–34 017, 2018.

[32] Y. B. Yang, C. Chen, W. Zhang, X. Deng, P. F. Du, H. L. Yang, W. D. Zhong, and L. Y. Chen, Secure and private NOMA VLC using OFDM with two-level chaotic encryption, *Opt. Express*, vol. 26, no. 26, pp. 34 031–34 042, 2018.

[33] B. J. Lin, Z. Ghassemlooy, X. Tang, Y. W. Li, and M. Zhang, Experimental demonstration of optical MIMO NOMA-VLC with single carrier transmission, *Opt. Commun.*, vol. 402, pp. 52–55, 2017.

[34] H. Marshoud, P. C. Sofotasios, S. Muhaidat, G. K. Karagiannidis, and B. S. Sharif, On the performance of visible light communication systems with non-orthogonal multiple access, *IEEE Trans. Wirel. Commun.*, vol. 16, no. 10, pp. 6350–6364, 2017.

[35] X. D. Liu, Z. Z. Chen, Y. H. Wang, F. H. Zhou, Y. S. Luo, and R. Q. Hu, BER analysis of NOMA-enabled visible light communication systems with different modulations, *IEEE Trans. Vehicul. Technol.*, vol. 68, no. 11, pp. 10 807–10 821, 2019.

[36] H. Y. Li, Z. T. Huang, Y. Xiao, S. Zhan, and Y. F. Ji, Solution for error propagation in a NOMA-based VLC network: Symmetric superposition coding, *Opt. Express*, vol. 25, no. 24, pp. 29 856–29 863, 2017.

[37] C. Chen, W. D. Zhong, H. L. Yang, P. F. Du, and Y. B. Yang, Flexible-rate SIC-free NOMA for downlink VLC based on constellation partitioning coding, *IEEE Wirel. Commun. Lett.*, vol. 8, no. 2, pp. 568–571, 2019.

[38] J. Shi, J. He, Y. Hong, and L. K. Chen, Performance-enhanced NOMA-VLC using subcarrier pairwise coding, *Opt. Commun.*, vol. 450, pp. 141–146, 2019.

[39] T. Cao, H. Zhang, and J. Song, BER performance analysis for downlink non-orthogonal multiple access with error propagation mitigated method in visible light communications, under review.

[40] Z. Ghassemlooy, W. Popoola, and S. Rajbhandari, *Optical Wireless Communications*: *System and Channel Modelling with Matlab®*. Bellingham, WA, USA: CRC Press, 2019.

[41] *IEEE Standard for Local and Metropolitan Area Networks–Part 15.7*: *Short-Range Optical Wireless Communications*, IEEE Std 802.15.7–2018, 2019.

[42] Z. Y. Wang, H. Y. Yu, and D. M. Wang, Channel and bit adaptive power control strategy for uplink NOMA VLC systems, *Appl. Sci.*, vol. 9, no. 2, p. 220, 2019.

[43] Z. Ghassemlooy, L. N. Alves, S. Zvanovec, and M. Ali Khalighi, Visible light communications: Theory and applications, Boca Raton, FL, USA: CRC Press, 2017.

[44] D. Zhou, T. Cao, Y. T. Yang, J. X. Zhang, P. Wang, and B. S. Yang, Symbol error rate performance analysis of soft-decision decoded MPPM free space optical system over exponentiated Weibull fading channels, *Chin. Opt. Lett.*, vol. 15, no. 5, p. 050602, 2017.

[45] T. M. Cover and J. A. Thomas, *Elements of Information Theory*, 2nd ed. New York, NY, USA: John Wiley & Sons, 2006.

[46] A. Papoulis, *Probability*, *Random Variables*, *and Stochastic Processes*. New York, NY, USA: McGraw–Hill, 1991.

**Tian Cao** received the BS and MS degrees in telecommunication engineering from Xidian University in 2014 and 2017, respectively. He is currently pursuing the PhD degree at the Department of Electronic Engineering, Tsinghua University. His research interests include ultraviolet communications and visible light communications.

**Hongming Zhang** is an associate professor at the Department of Electronic Engineering, Tsinghua University. He received the BS and PhD degrees from Tsinghua University in 1998 and 2003, respectively. He has applied for more than 20 invention patents in China, and published more than 80 research papers. His main research interests include visible light communication and indoor positioning technology.

**Jian Song** received the BEng and PhD degrees in electrical engineering from Tsinghua University in 1990 and 1995, respectively. He was with the Chinese University of Hong Kong and the University of Waterloo, Canada in 1996 and 1997, respectively. He worked for industry in U.S. for seven years. He joined the faculty team with Tsinghua University as a professor in 2005, where he is currently the director of the DTV Technology Research and Development Center, Tsinghua University. His research interests include digital television terrestrial broadcasting, wireless communication, power line communication, and visible light communication. He has published over 290 peer-reviewed journal and conference papers in the above areas and one book in DTV area by Wiley, holds two U.S. and over 70 Chinese patents. He was a recipient of the IEEE Scott Helt Memorial Award in 2015. He is a fellow of IET and CIE.